Catalysis Today 142 (2008) 61-69

In-Situ Investigation of Gas Phase Radical Chemistry in the Catalytic Partial Oxidation of Methane on Pt

M. Geske, K. Pelzer, R. Horn, F.C. Jentoft, R. Schlögl*

Fritz Haber Institute of the Max Planck Society, Department of Inorganic Chemistry, Faradayweg 4-6, 14195 Berlin, Germany

Available online 28 February 2009

Abstract

The catalytic partial oxidation of methane on platinum was studied in situ under atmospheric pressure and temperatures between 1000 and 1300 °C. By combining radical measurements using a molecular beam mass spectrometer and threshold ionization with GC, GC-MS and temperature profile measurements it was demonstrated that a homogeneous reaction pathway is opened at temperatures above 1100 °C, in parallel to heterogeneous reactions which start already at 600 °C. Before ignition of gas phase chemistry, only CO, H_2, CO_2 and H_2O are formed at the catalyst surface. Upon ignition of gas chemistry, CH_3· radicals, C2 coupling products and traces of C3 and C4 hydrocarbons are observed. Because the formation of CH_3· radicals correlates with the formation of C2 products it can be concluded that C2 products are formed by coupling of methyl radicals in the gas phase followed by dehydrogenation reactions. This formation pathway was predicted by numerical simulations and this work presents an experimental confirmation under high temperature atmospheric pressure conditions.

Keywords: catalytic partial oxidation, methane, platinum, methyl radical, molecular beam mass spectrometry, gas phase chemistry

1. Introduction

The presence of vast reserves of natural gas containing predominantly methane has encouraged scientific efforts to utilize it as chemical feedstock, alternatively to crude oil. Currently, research is directed to convert methane by catalytic partial oxidation (CPO) into i) synthesis gas (Eq. 1) [1], ii) ethylene (Eq. 2) [2], iii) formaldehyde (Eq. 3) [3] and iv) methanol (Eq. 4) [3]. Whereas methane CPO to formaldehyde and methanol is at the research stage and far from being commercially relevant (few % yields), methane CPO to ethylene (oxidative coupling) yields up to industrially interesting 25 % C2 yield (C_2H_6 + C_2H_4 + C_2H_2) [4] and methane CPO to syngas has reached pilot plant stage [1].

$$CH_4 + \tfrac{1}{2} O_2 \rightarrow CO + 2H_2 \qquad \Delta_r H° = -36 \text{ kJ/mol} \qquad (1)$$

$$CH_4 + \tfrac{1}{2} O_2 \rightarrow \tfrac{1}{2} C_2H_4 + H_2O \qquad \Delta_r H° = -185 \text{ kJ/mol} \qquad (2)$$

$$CH_4 + O_2 \rightarrow HCHO + H_2O \qquad \Delta_r H° = -320 \text{ kJ/mol} \qquad (3)$$

$$CH_4 + \tfrac{1}{2} O_2 \rightarrow CH_3OH \qquad \Delta_r H° = -164 \text{ kJ/mol} \qquad (4)$$

The motivation of the present work was to investigate the impact of gas phase chemistry on the methane oxidation on Pt because there is evidence in the literature that gas phase reactions play an important role for the above mentioned target transformations. In particular the focus is on the oxidative coupling of CH_4 to C2 species.

Catalytic methane oxidations and many other alkane oxidations are very exothermic and often very fast. In this situation heat generation is typically faster than heat losses by convection, conduction and radiation leading to high temperatures and interesting phenomena such as coupled surface-gas reactions, mass and heat transport limitations, ignition-extinction of surface chemistry, ignition-extinction of gas phase chemistry and autothermal reactor operation. Of particular interest is the exchange of radicals between the surface and the gas phase [5, 6]. As will be outlined in the following scattered experimental and numerical studies exist shedding light onto different aspects of methane oxidation and methane coupling on Pt but it is an open question whether these results can be extrapolated to high temperature (>1000 °C) and high pressure (>10^5 Pa) conditions [7, 8].

The surface chemistry of the methane oxidation on Pt has been studied extensively in the past and only the main results can be summarized here. Generally there is consent that CO, H_2, CO_2 and H_2O are the main surface reaction products with high selectivities to CO_2 and H_2O at low temperatures and to CO and H_2 at high temperatures [9-12]. It is always observed that the selectivity to H_2 increases more strongly with temperature than that of CO. A recent study reporting spatially resolved concentration and temperature profiles in a Pt foam catalyst gives an explanation of these general trends by showing that the methane CPO is a combination of exothermic total and partial oxidation reactions and endothermic reforming reactions [12]. In presence of gas phase oxygen at the beginning of the catalyst bed the reaction can be described by the stoichiometric equation (Eq. 5) in which x ($0 \le x \le 2$) and y ($0 \le y \le 1$) depend on the partial pressure of the reactants and the temperature.

$$CH_4 + (2\text{-}x/2\text{-}y/2)\ O_2 \rightarrow x\ H_2 + y\ CO + (2\text{-}x)H_2O + (1\text{-}y)\ CO_2 \quad (5)$$

At synthesis gas stoichiometry (C/O=1.0) and high temperatures (T>1000 °C), x and y are close to unity so that H_2, CO and H_2O are nearly formed in equimolar amounts whereas only small amounts of CO_2 are formed. After gas phase oxygen has been consumed, methane conversion continues with water as co-reactant meaning that steam reforming (Eq. 6) is the dominant reaction path

$$CH_4 + H_2O \rightarrow CO + 3H_2 \quad (6)$$

Whereas CO_2 reforming seems to be negligible under high temperature conditions, the water gas shift equilibrium (Eq. 7) might be another important reaction which contributes to the observed product distribution.

$$CO + H_2O \leftrightarrow CO_2 + H_2 \quad (7)$$

The surface chemistry of the methane oxidation on Pt has also been studied with respect to C2 formation and some mechanistic picture can be extracted, even though experimental conditions vary widely.

Somorjai et al. report methane dissociation on the least reactive Pt crystal face (111) at temperatures as low as 250 K [13] without evidence of the nature of the dissociation products. In a further study [14] over a temperature range from 300 K to 500 K and 1 Torr pressure, the authors report SFG and STM data showing the formation of CH_3 groups, carbon and hydrogen at the Pt surface. C-C coupling between CH_3 and C forming ethylidyne (C_2H_3) is reported at 400 K. Ethylidyne seems to be an intermediate because it dissociates at higher temperatures into C_2H and CH. The surface chemistry of CH_3 on Pt (111) was also studied by depositing CH_3 from gas phase pyrolysis of azomethane [15, 16]. In [15], the authors do not observe any coupling of two CH_3 species rather than a competition between hydrogenation to CH_4 and further decomposition to surface carbon. In [16] higher methyl coverages were realized and TDS measurements showed high temperature (350 to 650 K) H_2 desorption typical for decomposition of C_2H_x species. From this observation the authors conclude on C-C coupling at the Pt surface but probably by CH_x species with x<3. Results of dissociative methane adsorption by King et al. [17] on Pt (110) give indications of C-C coupling to C_2H above 500 K and high coverages. However, also these C2 species were found to decompose at temperatures above 650 K. It can be summarized that in absence of oxygen a narrow temperature range (400 K to 650 K) exists for C-C coupling on Pt, probably not by CH_3 but CH_x (x<3) species. However, all C2 products formed are labile and decompose at higher temperature.

More relevant for the present work are surface science studies with oxygen present at the Pt surface [10, 18]. The result of these studies is that no C2 formation is observed if molecular or atomic oxygen is present on the Pt surface. Under oxidizing conditions CO and CO_2 are the only carbon containing products. Also atmospheric pressure studies of the methane partial oxidation on Pt-coated monoliths [19] and on Pt and Pt/Rh gauzes [20] indicate that H_2, CO, H_2O and CO_2 are formed via surface reactions. In summary, oxidative coupling of C1 to C2 species on a Pt surface under methane partial oxidation conditions is very unlikely.

As there is a formation of C_2 products under high temperature conditions (T >1000 °C) where not only surface but also gas reactions can occur [20, 21] the question arises what role platinum plays in this case. It is not clear how the platinum surface influences gas phase radical chain reactions and, with view on the oxidative coupling of methane on oxide catalysts, whether radicals desorb from the Pt surface.

As reviewed by Mackie [22], the relative concentration and the rate by which key radical species (e.g. H·, R·, RO·, RO_2·, HO_2·, and OH· (R = organic rest)) react in the gas phase determines whether coupling products, oxygenates or total oxidation products are formed. Generally, gas phase radical reactions are unselective leading to the thermodynamic stable products under reaction conditions and their rate increase with pressure because of the increasing collision frequency among the gas molecules.

A numerical study by Deutschmann and Schmidt [19] showed, that at pressures of 1 MPa and a catalyst temperature of 1188 K, gas phase chemistry downstream the catalyst foam starts to influence the ratio between partial oxidation products (H_2, CO) and total oxidation products (CO_2 and H_2O). It was found that downstream gas phase chemistry shifts the product distribution towards CO_2 and H_2O, reducing the syngas selectivity by about 2 %.

Very pronounced seems the impact of gas phase chemistry on the formation of C2 coupling products C_2H_6, C_2H_4, C_2H_2. Numerical studies on a Pt-gauze catalyst report C2 product formation downstream the gauze [23, 24]. By coupling a microkinetic surface model with a microkinetic gas phase model this C2 formation was attributed to coupling of CH_3· radicals in the gas phase [23, 24]. Even

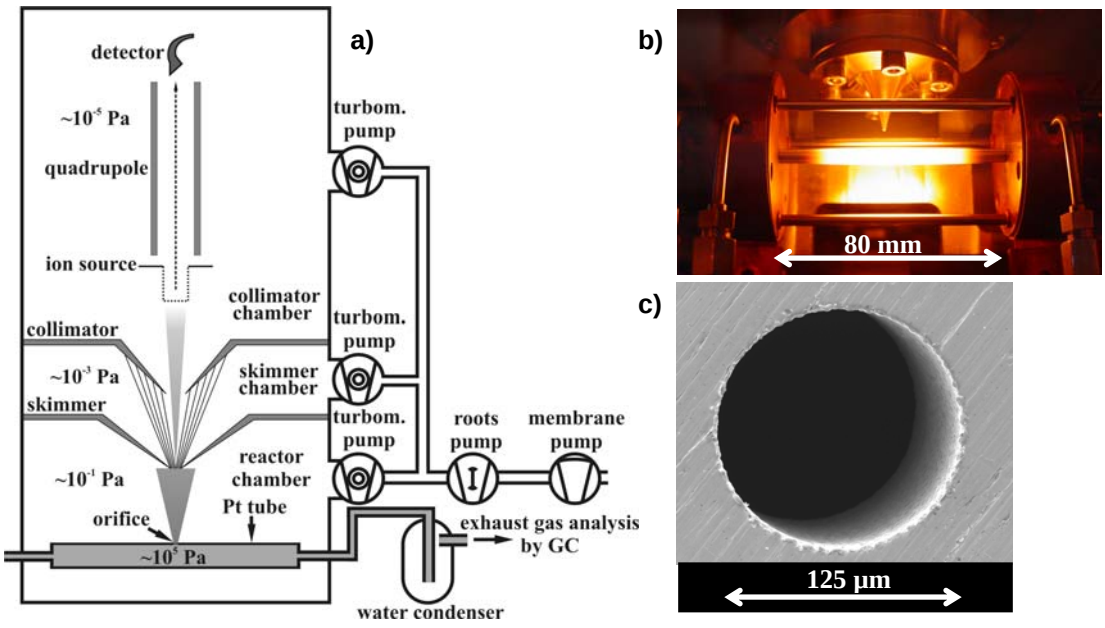

Fig. 1: a) Scheme of the MBMS set up, b) reactor under operation and c) image of the orifice

though there is no experimental proof, the simulations in [23, 24] indicate that methyl radicals do not desorb from the catalyst surface but are created in pure gas phase reactions downstream the gauze. This numerical result is in line with matrix isolation EPR studies by Lunsford et al. which verified the absence of CH_3· desorption from Pt [25] up to temperatures of 900 °C. It seems that Pt behaves differently than strong basic oxide catalysts (e.g. MgO, La_2O_3,) from which CH_3· radicals desorb into the gas phase as shown by matrix isolation EPR and photoionization mass spectrometry [2, 26]. What has been experimentally verified on Pt is the presence of OH· radicals over the Pt surface during methane oxidation using laser induced fluorescence spectroscopy [27]. According to [27] where the LIF studies were also complemented by numerical simulations, the OH· radicals originate from purely homogeneous reactions and the gas phase chemistry is rather suppressed by Pt than supported. In an earlier LIF study by Marks and Schmidt also OH· desorption was observed [28].

It can be summarized that the high rate by which the methane oxidation proceeds over many catalysts, coupled with a high rate of heat generation leads to a complicated non-linear network of surface and gas reactions. Surface and gas chemistry are coupled by mass and heat transport which are often slower than the chemical reactions. Apart from scattered experimental results and numerical predictions, not much is known about the interplay between surface and gas chemistry during partial oxidation of methane on Pt. The present work presents a first in-situ investigation of the radical chemistry in the gas phase for the methane oxidation on Pt under partial oxidation conditions (C/O = 0.6), atmospheric pressure and temperatures up to 1300 °C.

2. Experimental

2-1- Reactor and MBMS

The use of a Molecular Beam Mass Spectrometer (MBMS) equipped with a high temperature catalytic wall reactor [21] allows studying the methane CPO in situ. The setup is shown schematically in Fig. 1a. The catalytic wall reactor consists of a platinum tube (99.95 % purity, Ögussa, length = 100 mm, ID = 4.4 mm, OD = 5.0 mm) placed between two cooled copper clamps inside a vacuum chamber. The reactor was fed with a gas mixture of 490 ml/min methane, 410 ml/min oxygen and 100 ml/min inert gas as internal standard (Ar or He), resulting in a total flow of 1000 ml/min (STP conditions). Typically the feed stoichiometry is characterized by the C/O ratio, which is the ratio of carbon to oxygen atoms in the feed. The used mixture corresponds to a C/O ratio of 0.6. Gases were supplied from storage cylinders via mass flow controllers (CH_4 (99.95 %), O_2 (99.999 %), He (99.999 %), H_2 (99.999 %), Ar (99.999 %) and synthetic air (99.999 %), all Westfalen).

The reaction is started by passing an electric current through the tube leading to resistive heating. Once the reaction started at around 600 °C, it can run autothermally, or, with extra heating, at temperatures up to 1300 °C (Fig. 1b). All experiments were conducted at pressures close to atmospheric (104 to 113 kPa). The outer tube wall is kept under vacuum in the reactor chamber (approx. 10^{-1} Pa under operation). A small gas portion is sampled directly from above the reacting surface and expanded through an orifice (Ø 125 µm, Fig. 1c in the middle of the Pt reactor wall) into a three stage pumped vacuum background. The collision frequency between the molecules inside this free jet expansion drops to zero within microseconds preventing further reaction. An arrangement of differentially pumped skimmer

and collimator cones forms a molecular beam axially aligned with the mass spectrometer.

The quadrupole mass spectrometer (QMS, HAL IV Epic Hiden) allows analysis of the gas components in the formed molecular beam. Radicals can be selectively detected in presence of interfering species (same m/z) by threshold ionization. Here, the energy of the ionizing electrons is adjusted high enough to ionize the radical but lower than the appearance energy (fragmentation) from other molecules [29, 30].

Axial temperature profiles of the tube reactor are measured by line scanning optical pyrometry (IMPAC – IGAR 12-LO ratio pyrometer). Fast scanning, by using a mirror and a small angle step motor (0.45 ° per step), allows recording temperatures approximately every 4 mm. The stepper motor is controlled by a Lab View program. All temperature values reported in this work are maxima of the corresponding profiles. After water removal in a reflux condenser, the reactor exhaust product composition is analyzed by on-line GC and GC-MS. The gas chromatograph (Varian CP-3800) is equipped with two columns (Molsieve and Hayesep S). During sample injection both columns are connected in series. All gases enter at first the Hayesep S column where the hydrocarbons and CO_2 are retained and inert gases, oxygen and CO reach the Molsieve column. After this pre-separation, the columns are switched to a parallel mode and the effluent substances are analyzed. Inorganic compounds are detected by a thermal conductivity detector (TCD) and hydrocarbons are measured with a flame ionization detector (FID).

For the GC-MS analysis a second MS (Omnistar – Pfeiffer Vacuum) is connected directly in front of the TCD inlet. The scan time for a complete MS spectrum (1 to 80 amu) is with approx. 4 s much smaller than the FWHM of the analyzed GC peaks (10 s).

2.2. GC-quantification

The analysis of the exhaust gases of the reactor is performed without internal standard, because neither Ar nor He can be used with the GC. Ar and O_2 overlap in the Molsieve column and He is used as carrier gas. N_2 can not be used as internal standard because it interferes with CO in the MS.

Instead, the quantification is performed by using the known molecular inlet flows $F_{CH_4}^{in}$ and $F_{O_2}^{in}$.

Under the conditions used the deposition of carbon in the reactor and the formation of condensable oxygenates is virtually zero (steady state). Therefore a carbon atom balance with F denoting a molar flow rate gives:

$$F_C^{in} = F_C^{out} = F_{CH_4}^{in} \quad (8)$$

As every carbon containing species ($_X$) can be detected by the GC the total C amount is given by:

$$C_C^{ges} = \sum \nu_X C_X \quad (9)$$

(C = concentration in Vol%, ν = number of C atoms in X)
Individual flow rates for every carbon containing species can be calculated using:

$$F_X = \frac{F_C^{in}}{C_C^{ges}} \cdot C_X \quad (10)$$

Assuming ideal gases, the flow rate of the non C containing molecules (O_2 and H_2) can be calculated from:

$$F_{O_2} = \frac{F_C^{in}}{C_C^{ges}} \cdot C_{O_2} \quad (11)$$

The molar flow rate of water is calculated from an oxygen atom balance:

$$F_{H_2O}^{out} = 2 \cdot F_{O_2}^{in} - F_{CO}^{out} - 2 \cdot F_{CO_2}^{out} - 2 \cdot F_{O_2}^{out} \quad (12)$$

With all flow rates known the selectivities (S) and conversions (X) can be determined:

$$S_X = \frac{F_X \cdot \nu_X}{(F_{CH_4}^{in} - F_{CH_4}^{out})} \quad (13)$$

and

$$X_{CH_4} = \frac{F_{CH_4}^{out}}{(F_{CH_4}^{in} - F_{CH_4}^{out})} \quad (14)$$

2.3. Radical Measurements

2.3.1.Electron Energy Spread and Offset

To determine the onset of the gradually increasing ion signal in threshold ionization measurements, the energy spread and the energy offset of the ionizing electrons have to be determined. In an earlier publication [21], the authors showed that the energy spread of the ion source used in the molecular beam mass spectrometer is Gaussian and any measured ionization efficiency curve, is a convolution between this Gaussian energy spread function and the true but in most cases unknown ionization efficiency curve $P_i(E)$. As the single ionization of atoms close to the threshold can be approximated by Wannier's threshold law Eq. (15) [31], the ionization efficiency curve for the single ionization of Ar at 40 amu was measured from 15.0 to 17.5 eV and energy spread and offset were obtained by a nonlinear fit of the discretized convolution integral Eq. (16) to the threshold data (Fig. 2). In Eq. (16), i(V) is the measured ionization efficiency curve (ion signal vs. set electron energy V), C a proportionality constant, σ the standard deviation of the Gaussian energy spread, j the summation index and IP the

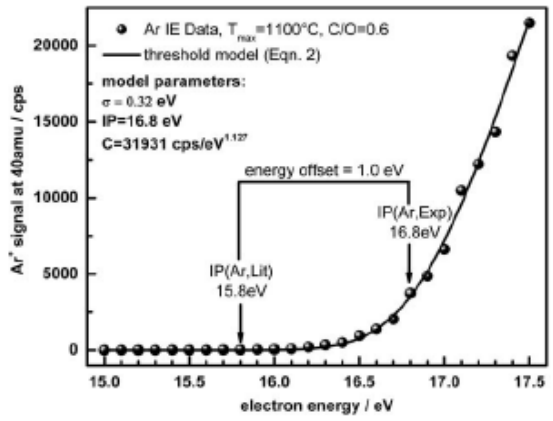

Fig. 2: Experimental threshold data for Ar single ionization (globes) and nonlinear fit of Eq.() (solid line) to determine the electron energy spread and offset [32]

offset shifted ionization potential of Ar. The summation starts at the ionization potential because there is no ionization, i.e. $P_i(E) = 0$, for electron energies lower than the ionization potential. As the ion source allows energy steps of 0.1 eV, ΔE was chosen to be 0.1. For a more detailed description of this procedure the reader is referred to [21].

$$P_i(E) = C \cdot (E - IP)^{1.127} \quad E \geq IP \tag{15}$$

$$i(V) = \frac{C}{\sigma\sqrt{2\pi}} \sum_{j=0}^{\infty} Exp\left(-\frac{(IP + j \cdot \Delta E - V)^2}{2\sigma^2} \right) \cdot (j \cdot \Delta E)^{1.127} \cdot \Delta E \tag{16}$$

The threshold ionization measurements of the internal standard Ar have been repeated for different reaction conditions. The slopes of the IE curves were found to depend on composition and temperature conditions in the reactor whereas electron energy offset and spread remain essentially constant. This can be understood because the slope of the IE curve depends on the Ar flow through the sampling orifice, which changes with changing experimental conditions, whereas energy spread and offset depend only on the ionizer in the mass spectrometer and not on the reactor conditions. On average, the electron energy offset was found to be 1.1 eV and the energy spread σ = 0.31 eV. This means that radicals can be selectively detected with the MBMS if the appearance potential of any interfering ion is at least 2σ = 0.62 eV higher than the ionization potential of the radical. The ionization potential of the target radical CH_3· is IP(CH_3·) = 9.84 eV [33]. By means of thermodynamics it can be shown that the appearance potential of CH_3^+ from any interfering ion AP(CH_3^+/CH_3-R), where R is an organic rest, must always be higher than IP(CH_3·) namely by the bond dissociation enthalpy of the R-CH_3 bond which is typically of the order of 3 to 4 eV [30]. For example, AP(CH_3^+/CH_4) = 14.01 eV [34] and AP(CH_3^+/C_2H_6) = 13.65 eV [35]. Therefore it should be possible to detect CH_3· radicals in presence of any interfering hydrocarbon molecule.

2.3.2. Radical Quantification

The method of radical quantification used in this work is based on the work of Singh, Coburn and Graves [36]. In this method, radicals are quantified by reference to an ion which is the product of a direct ionization process rather than a fragment and lies very close in mass to the radical ion (e.g. CH_4^+ for the radical ion CH_3^+). This ensures similar extraction efficiencies in the ionizer, similar quadrupole transmissions and similar detector sensitivities for both ions. If the signal of the stable ion (e.g. CH_4^+) can be related to a concentration measure of its parent molecule in the reactor tube (CH_4), it is possible to calculate the concentration of the radical in the reactor. Eq. (17) shows the applied relationship for the quantification of CH_3· radicals in this work. The radical concentration is obtained in units of a molar flow rate F, as it is based on the methane molar flow rate at the orifice position, which itself is calculated from the known molar flow rate of the inert standard Ar. The other symbols in Eq. (17) are A, the slope of the ion signal close to the threshold; λ, the slope of the ionization cross section at the threshold (e.g. from NIST database [37, 38]); S, the mass spectrometer signal at an energy where Ar and CH_4 ionize (in this work 25 eV) and R, the response factor for the mass spectrometric detection of the stable ion (CH_4^+) based on the internal standard Ar. The slope was used in this case instead of individual ionization cross sections to minimize the error.

$$F_{CH_3\cdot} = \frac{A^{CH_3\cdot \rightarrow CH_3^+} \cdot \lambda^{CH_4 \rightarrow CH_4^+}}{A^{CH_4 \rightarrow CH_4^+} \cdot \lambda^{CH_3\cdot \rightarrow CH_3^+}} \cdot F_{Ar}^{in} \cdot \frac{S_{CH_4}^{25eV}}{S_{Ar}^{25eV} \cdot R_{CH_4/Ar}^{cal}} \tag{17}$$

Because the molecular beam formation from a free jet expansion is a very complex process the error bar for this quantification method can not yet been specified. Dedicated experiments indicate a strong and complicated dependence of the mass spectrometer signal on species concentration, temperature and pressure in the reactor and on the orifice-skimmer distance. Further experiments are necessary to investigate how these variables influence species of different mass (e.g. CH_4 and Ar) which determines the error of the quantification procedure. Currently, CH_4 and Ar are considered to behave the same in the molecular beam forming process. However, the order of magnitude of the calculated CH_3· radical flow rates agrees with preliminary numerical simulations performed on the reactor using the CRESLAF code in CHEMKIN (not yet published).

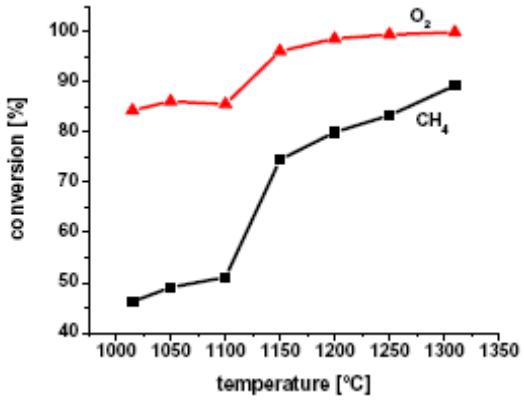

Fig. 3: Conversion of reactants during CPO of methane depending on T

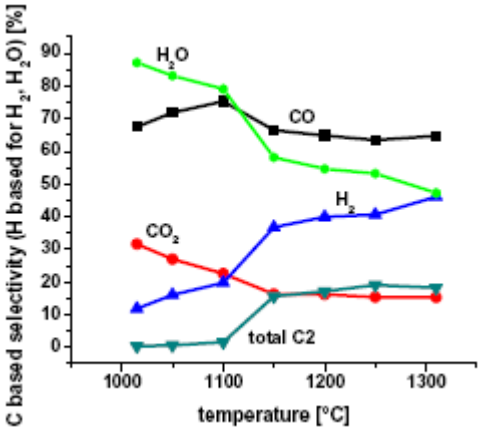

Fig. 4: Selectivities of products during methane CPO

3. Results

3.1. Catalytic Data

At temperatures lower than about 1100 °C, unconverted methane and oxygen were found by on line GC analysis of the reactor effluent stream (Fig. 3). A significant increase of the reactant conversion is noticed by increasing the temperature above 1100 °C. Upon increasing the temperature by only 50 °C from 1100 to 1150 °C, the O_2 conversion increases in a step like manner from 85 to 95 % whereas methane conversion increases from 50 to 75 %. Upon further heating, the O_2 conversion rises slowly to 100 % whereas the CH_4 conversion increases linearly to about 90 %.

Below 1100 °C, the reaction products are mainly H_2, CO, H_2O and CO_2 formed by oxidation reactions, reforming reactions and water gas shift as discussed in the introduction. CO and H_2O dominate and only traces of ethane are formed as C2 coupling products (Fig. 4). The step like change in conversion observed upon heating from 1100 to 1150 °C is also reflected in the selectivity patterns. Both, the selectivity to H_2 and C2 show a step like increase from 20 to 35 % and ~0 to 15 % respectively. C2 formation increases at the expense of CO and CO_2 formation, for which the selectivity drops.

As the temperature is increased from 1150 to 1300°C, the selectivity to H_2 and C2 rises further and those of H_2O, CO and CO_2 drop but not as steeply as between 1100-1150 °C.

After the sharp temperature rise from 1100 to 1150 °C, not only ethane, ethylene and acetylene are suddenly detected by GC, also small but noticeable amounts of higher unsaturated hydrocarbons. Several of these species could be identified by GC-MS and comparison with literature data from NIST [37] and reference chromatograms [39]. Four examples are presented in Fig. 5. The peaks marked with stars arise from water eluting from the column and the MS background (N_2, O_2, CO_2, Ar). The background signal of the other masses is stable between 0.5 and $1 \cdot 10^{-11}$ Amperes and therefore five times lower than the smallest studied peak. A list with all identified coupling products with their maximal achieved selectivities is given in Tab. 1. At temperatures around 1310°C, noticeable amounts of benzene are formed, a typical coke precursor. Indeed, higher C/O ratios than 0.6 could not be investigated at such high temperatures as coke formation caused a plugging of the sampling orifice.

Tab. 1: Maximal concentrations of detected higher hydrocarbons depending on the temperature during methane CPO

Hydrocarbon	max. selectivity / %	at T / °C
Acetylene	17.2	1310
Ethylene	4.4	1150
Ethane	1.5	1150
Allene	0.2	1200
Propyne	0.5	1200
1-Butene-3-yne	0.3	1200
1,3-Butadiyne	0.8	1310
Benzene	0.7	1310

3.2. Radical Measurements during Methane CPO

With the appearance of C2 and other coupling products at temperatures ≥ 1150 °C also methyl radicals are detected. In Fig. 6, mass spectra and IE curves are compared for 1015 and 1310 °C. At 1015 °C, the onset of the IE curve is at 14 eV, which corresponds to the appearance potential of CH_3^+ from CH_4 (14.01 eV) [34]. The inset in the left side of Fig. 6 shows the mass spectrum at an ionizing energy of 11.9 eV. The peak at 15 amu is close to zero, as there are no $CH_3\cdot$ radicals and methane does not dissociate at this low energy. At 1310 °C, the IE curve increases from 9.8 eV on, a clear indication of $CH_3\cdot$ radicals

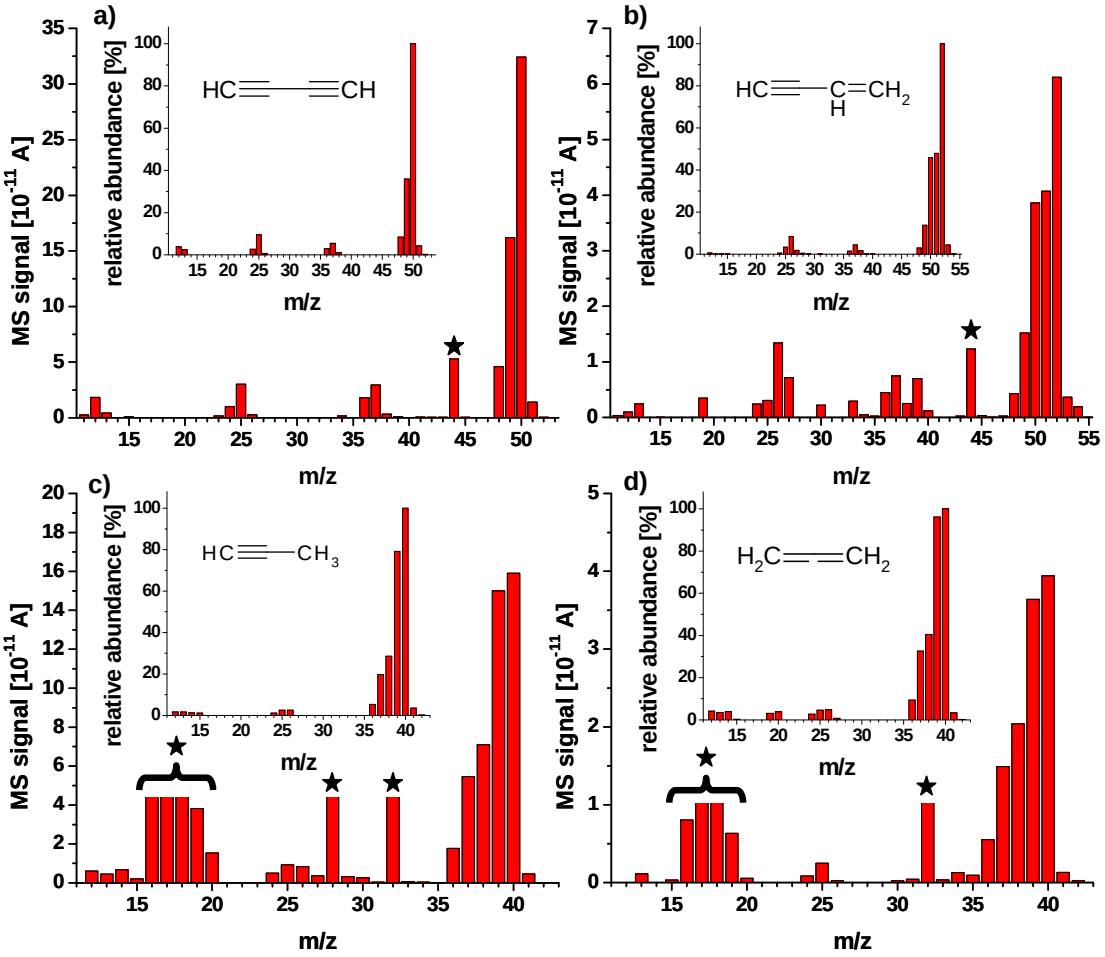

Fig. 5: Four unsaturated hydrocarbons identified by GC-MS. a) 1,3-butadiyne; b) 1-buten-3-yne; c) propyne; d) allene. The insets present the NIST data [37] for comparison.

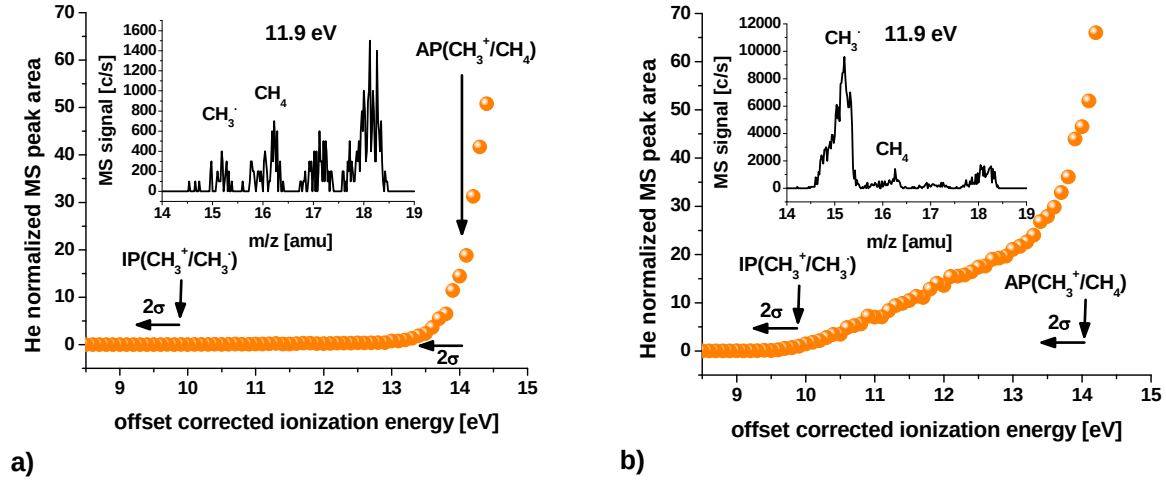

Fig. 6: IE curves at 15 amu for the detection of CH3· radicals by threshold ionization at a) 1015 °C and b) 1310 °C

($IP(CH_3^+/CH_3\cdot)$ = 9.84 eV) [33]. At higher electron energies the curve increases even more steeply caused by CH_3^+ fragment formation from methane at 14 eV. Without $CH_3\cdot$ radicals (1015 °C), the IE curve remains close to zero until the fragmentation processes begin. The inset at the right side of Fig. 6 shows again the mass spectrum at 11.9 eV ionizing energy. Now $CH_3\cdot$ radicals produce a strong signal at 15 amu whereas CH_4 is barely ionized at 16 amu without dissociation to CH_3^+.

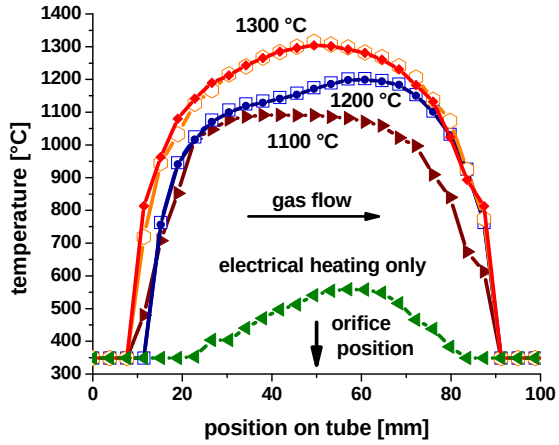

Fig. 7: Axial temperature profiles of the Pt wall reactor with electrical heating only and during operation at 1100 °C, 1200 °C and 1300 °C

3.3. Temperature Profiles

Line scanning pyrometry allows contact-free measurement of temperature profiles across the Pt tube during methane CPO. Changes in the temperature profiles upon ignition or increase of the heating current can be correlated with the product gas composition from the QMS and GC-MS measurements to give a more detailed view of mechanistic changes.

Under all conditions, the tube ends are cold and the hot zone is confined to the middle of the tube with a length of about 70 to 80 mm (Fig. 1b). At C/O = 0.6, the methane CPO ignites typically around 600 °C. If the reaction runs autothermally at C/O = 0.6, a maximum temperature of about 1000 °C is reached. The tube temperature is further increased by electric heating, reaching 1100 °C (23 W), 1200 °C (139 W) and 1300 °C (225 W) as shown in Fig. 7. The temperature profile of the tube for a particular C/O ratio is very reproducible, i.e. the same profile is measured after switching back from experiments at other C/O ratios. This is illustrated in Fig. 7, where two profiles at 1200 °C and two profiles at 1300 °C are superimposed which have been measured at intervals of 30 min. This reproducibility indicates that the reactor reaches steady state quickly.

The temperature profile of the heated tube without gas flow (not shown) is symmetric with a maximum in the tube center as can be expected for electric heating of an ohmic resistor. With gas flow, but without reaction, the heat is convectively transported within the stream towards the outlet, shifting the temperature maximum in the same direction ("electrical heating only"). When sufficient heating power is provided, oxidation reactions start at the platinum surface. The heat liberated causes a self-acceleration of these exothermic surface reactions, more heat is liberated and reactor light-off is observed. The reaction zone proceeds towards the reactor inlet where fresh reactants enter. Between autothermal reactor operation and the ignition of gas phase chemistry electrical heating and surface reactions result in a temperature profile with a 40mm wide, slightly declining plateau extending from 30mm to 70mm axial coordinates. The gradual temperature decrease in this section might be due to chemical cooling by endothermic steam reforming. Only CO, CO_2, H_2 and H_2O are the products in this surface chemistry regime in agreement with the literature.

Between 1100 °C and 1200 °C a second ignition behavior is observed leading to a temperature maximum located towards the tube outlet. Further electrical heating up to 1300 °C leads to a symmetrical temperature profile with the maximum in the tube center.

4. Discussion

The following picture of the methane CPO in the reactor can be derived combining catalytic results, mass spectrometric radical measurements and temperature profiles. Around 600 °C the reactor lights-off by ignition of surface reactions. This value is in good agreement with literature values for surface ignition of CH_4/O_2 mixtures on Pt at C/O = 0.6 [40]. The autothermal operation temperature at C/O = 0.6 is around 1000 °C. Between autothermal operation and heating to 1100 °C, exothermic surface reactions dominate the reaction network. In agreement with the literature [19] H_2, CO, H_2O and CO_2 are found as the main products which are probably formed by total oxidation, partial oxidation, steam reforming and water gas shift [12]. No radicals are detected indicating gas phase chemistry. O_2 conversion is incomplete under these conditions which is not surprising because the ratio of residence time in the reactor to diffusion time from the tube center to the wall is close to unity. Together with the laminar flow profile (Reynolds number is estimated from 100 to 400 depending on the reaction conditions) some methane and oxygen remain unconverted in the bulk gas phase as they do not come in contact with the Pt surface.

If the heating power is further increased to raise the temperature above 1100 °C, a second ignition behavior is observed and the temperature profile of the reactor develops a pronounced maximum located towards the outlet indicating a strong additional heat release (e.g. 1200 °C curve in Fig. 7). This second ignition point is further characterized by a step like increase in O_2 and CH_4 conversion (O_2 conversion approaches completion), the formation of C2 coupling products and the detection of CH_3· radicals. In light of numerical simulations published in the literature [5], this second ignition can be attributed to the ignition of gas phase reactions. The ignition temperature of the gas phase reactions (~1150 °C) is much higher than the ignition temperature of the catalytic reactions (~600 °C) because gas phase reactions have much higher activation barriers. Another cause of the delayed gas phase ignition might be that the gas temperature is lower than the surface temperature due to the finite rate of heat transport from the surface to the gas phase causing a slower rise of the gas phase temperature compared to the surface temperature. Also chemi

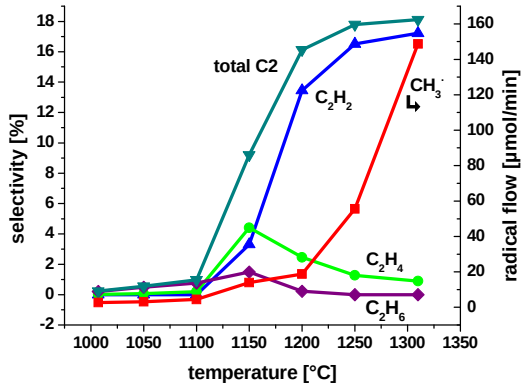

Fig. 8: Selectivities of ethane, ethylene and acetylene and comparison of CH_3· flows depending on the temperature

cal reasons (e.g. radical exchange) might influence the start of gas phase reactions.

Fig. 8 displays the selectivity for the formation of the C2 coupling products (total C2, ethane, ethylene, acetylene) as well as the molar flow rate of CH_3· radicals in dependence of the temperature.

There is a correlation between the formation of CH_3· radicals and the formation of C2 coupling products. The more CH_3· radicals are produced, the more C2 coupling products are formed. This finding indicates that C2 coupling products originate from a recombination of CH_3· radicals in the gas phase (Eq. 18). This is the first experimental verification of the numerical predictions by Quiceno et al. [20, 23]

$$CH_3\cdot + CH_3\cdot \rightarrow C_2H_6 \qquad (18)$$

The different shapes of the CH_3· radical curve and the total C2 formation curve result from the different sampling positions. While CH_3· radicals are measured in the middle of the tube, C2 products are measured at the tube exit (see Fig. 1).

The fact that small amounts of ethane but no CH_3· radicals are observed between the autothermal temperature of 1000 °C and the gas phase ignition point at around 1150 °C can be explained by a CH_3· concentration below the detection limit of the method (low ppm range [21]). In light of the discussion of surface chemistry in the introduction it is not likely that C2 coupling products are formed on the Pt surface. The small ethane formation before gas phase ignition is rather due to coupling of CH_3· radicals which are part of the radical pool formed by homogeneous reactions before ignition. Between 1000 and 1100 °C the main C2 product is ethane, at 1150 °C ethylene and at all higher temperatures acetylene in agreement with the thermodynamic trend [41]. As CH_2· or CH· radicals are not observed in the gas phase the formation of ethylene and acetylene does not occur by coupling of the aforementioned species but rather by dehydrogenation or oxidative dehydrogenation of ethane. This is also the common interpretation in the literature [42, 43].

$$C_2H_6 \rightarrow C_2H_4 + H_2 \rightarrow C_2H_2 + 2H_2 \qquad (19)$$

or

$$C_2H_6 + O_2 \rightarrow C_2H_4 + H_2O + \tfrac{1}{2}\,O_2 \rightarrow C_2H_2 + 2H_2O \qquad (20)$$

If direct coupling of CH_2· or CH· was the formation mechanism to C_2H_4 and C_2H_2 respectively the species should be detected facing the high concentrations by which ethylene and in particular acetylene, are formed.

Similar to EPR results of Lunsford and coworkers [25], also the data in this work are in favor of an exclusive homogeneous generation of CH_3 radicals during methane oxidation without CH_3 desorption from the Pt surface. It is not plausible that an increase in temperature by 50 °C from 1100 to 1150 °C leads suddenly to a production and desorption of CH_3· radicals from the surface. It is more likely that methyl radicals arise predominantly from gas phase reactions, initiated and sustained by heat release from the Pt surface. This interpretation would also be in agreement with the numerical predictions of Quiceno et al. [23, 24] showing that CH_3 radicals are rather consumed than produced by a Pt surface. Pt is an extremely active oxidation catalyst and it is unlikely that an alkyl radical can desorb from the surface without being converted to CO or CO_2. The lack of CH_3 desorption is a clear difference between Pt and typical oxidative coupling catalysts like Li/MgO or La_2O_3 where CH_3· radical desorption plays a vital role in the mechanism [44, 45].

Whether OH· radicals exist in the gas phase, as reported in the literature based on LIF results [27, 28], can not be inferred from the measurements. With large amounts of CH_4 in the molecular beam it is impossible to measure OH· by threshold ionization because ionization of methane molecules containing ^{13}C dominates the signal at 17 amu ($^{13}C^1H_4$). Methane ionizes at lower energies (IP(CH_4) = 12.6 eV [34]) than OH radicals (13.2 eV [46]).

Other radicals that are typical for gas phase alkane oxidation reactions like O·, HO_2·, H·, RO· and RO_2· can be measured with the MBMS but were not detected under any of the investigated conditions. Also Pt_xO_y species, which could be potential initiators of gas phase chemistry, were not detected in the gas phase using full mass scans up to 510 amu. Combining these results with information from the literature [47] it can be suggested that methyl radicals are created homogeneously in the gas phase by one of the following reactions:

$$CH_4 + O_2 \rightarrow CH_3 + HO_2 \qquad (21)$$
$$CH_4 + M \rightarrow CH_3 + H + M \qquad (22)$$
$$CH_4 + OH \rightarrow CH_3 + H_2O \qquad (23)$$

In Eq. (22), M denotes an inert collision partner like for example Ar.

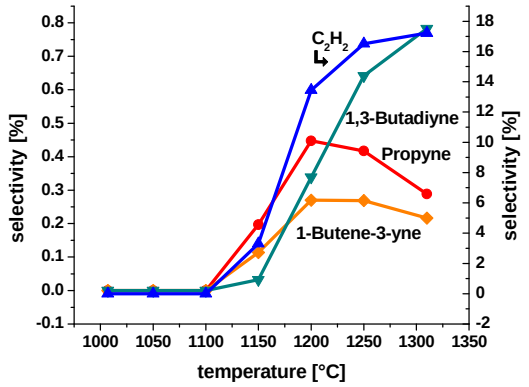

Fig. 9: Selectivities of C3 and C4 hydrocarbons in dependence of the acetylene formation

That fact that no other radicals than CH_3· are observed does not mean that no other radicals are involved in the gas phase oxidation of methane it rather means that the other radicals react away so quickly that their steady state concentration is below the detection limit of the method (low ppm range [21]).

Obviously, CH_3· radicals are comparably stable [48] and formed in large quantities compared to all other radical species in the reaction network. Indeed, the numerical simulations of the methane CPO on a Pt gauze by Quiceno et al. [24] show that CH_3· radicals downstream the gauze have a higher concentration than HO_2 and OH.

The hypothesis, that the second reaction light off between 1100 °C and 1150 °C is due to gas phase radical chemistry, is further supported by the observation of C3 and C4 coupling products. Various unsaturated higher hydrocarbons (C_3H_4, C_4H_4 and C_4H_2) were identified in the reactor outlet by GC-MS; however, their concentrations never exceeded a few ppm. It can be expected that the formation mechanism of these products is similar to that for the C2 coupling products meaning that C3 products are formed by recombination of methyl and C2 alkyl whereas C4 products are formed either by recombination of methyl with C3 alkyl or two C2 alkyl radicals. At temperatures ≥ 1250 °C, 1,3-butadiyne (diacetylene) is the major C4 product (Fig. 9). The gas phase formation of C3 and C4 coupling products is also in line with literature results. By combining isotope tracer experiments and numerical simulations, Mims et al. [49] traced the homogeneous coupling chemistry during methane oxidative coupling with focus on C3 and C4 formation. They found the higher hydrocarbon growth occurs through gas-phase radical reactions with little interference by the catalyst.

5. Conclusion

By combining in-situ measurements of CH_3· radicals during methane catalytic partial oxidation on Pt with GC analysis of the reactor off-gases and temperature profile measurements of the reactor tube it was shown that the methane CPO proceeds via a heterogeneous-homogeneous mechanism. At C/O = 0.6, ignition of surface chemistry is observed at around 600 °C leading to autothermal operation at 1000 °C. From autothermal operation up to T ≈ 1100 °C, oxygen conversion is incomplete and surface oxidation reactions to CO, H_2, CO_2 and H_2O dominate. No radicals are detected by threshold ionization indicating the absence of gas phase chemistry. If the temperature is increased above 1100 °C an ignition is observed accompanied by complete oxygen conversion, detection of CH_3· radicals, significant amounts of C2 coupling products and traces of C3 and C4 coupling products. This second ignition is attributed to exothermic gas phase radical chemistry. The measurements presented in this work provide the first experimental correlation between CH_3· radical formation and formation of C2 products under high temperature and atmospheric pressure condition and confirm numerical predictions in the literature [23, 24]. In contrast to the methane oxidative coupling on strong basic oxides like Li/MgO, the role of Pt is not to generate CH_3· radicals which desorb into the gas phase rather than to supply the necessary heat to initiate and sustain the radical forming gas phase chemistry.

Acknowledgements

The authors thank J. Ihmann for support during the construction phase of the high temperature reactor and A. Taha for setting up the pyrometer temperature measurements.

References

[1] A.P.E. York, T.-c. Xiao, M.L.H. Green and J.B. Claridge, Catal. Rev., 49 (2007) 511.
[2] J.H. Lunsford, Angew. Chem. Int. Ed. Engl., 34 (1995) 970.
[3] K. Tabata, Y. Teng, T. Takemoto and E. Suzuki, Catal. Rev., 44 (2002) 1.
[4] G.J. Hutchings, M.S. Scurrell and J.R. Woodhouse, Chem. Soc. Rev., 18 (1989) 251.
[5] R.J. Olsen, W.R. Williams, X. Song and L.D. Schmidt, Chem. Eng. Sci., 47 (1992) 2505.
[6] S. Chattopadhyay and G. Veser, AIChE J., 52 (2006) 2217.
[7] D.J. Discroll, K.D. Campbell and J.H. Lunsford, Adv. Catal., 35 (1987) 139.
[8] T.A. Garibyan and L.Y. Margolis, Catal. Rev.-Sci. Eng., 31 (1989) 335.
[9] D.A. Hickman and L.D. Schmidt, Science, 259 (1993) 343.
[10] D.T.P. Watson, J.J.W. Harris and D.A. King, J. Phys. Chem. B, 106 (2002) 3416.

[11] S.F. Rice, A.H. McDaniel, E.S. Hecht and A.J.J. Hardy, Ind. Eng. Chem. Res., 46 (2007) 1114.
[12] R. Horn, K.A. Williams, N.J. Degenstein, A.B. Larsen, D.D. Nogare, S.A. Tupy and L.D. Schmidt, Journal of Catalysis, 249 (2007).
[13] G.A. Somorjai and A.L. Marsh, Phil. Trans. R. Soc. A, 363 (2005) 879.
[14] A.L. Marsh, K.A. Becraft and G.A. Somorjai, J. Phys. Chem. B, 109 (2005) 13619.
[15] D.H. Fairbrother, X.D. Peng, M. Trenary and P.C. Stair, J. Chem. Soc., Faraday Trans., 91 (1995) 3619.
[16] D.H. Fairbrother, X.D. Peng, R. Viswanathan and P.C. Stair, Surf. Sci. Lett., 285 (1993).
[17] D.T.P. Watson, S. Titmuss and D.A. King, Surf. Sci., 505 (2002) 49.
[18] M. Valden, N. Xiang, J. Pere and M. Pessa, Appl. Surf. Sci., 99 (1996) 83.
[19] O. Deutschmann and L.D. Schmidt, AIChE J., 44 (1998) 2465.
[20] K.H. Hofstad, T. Sperle, O.A. Rokstad and A. Holmen, Catal. Lett., 45 (1997) 97.
[21] R. Horn, K. Ihmann, J. Ihmann, F.C. Jentoft, M. Geske, A. Taha, K. Pelzer and R. Schlögl, Rev. Sci. Instrum., 77 (2006) 9.
[22] J.C. Mackie, Catal. Rev.-Sci. Eng., 33 (1991) 169
[23] R. Quiceno, O. Deutschmann, J. Warnatz and J. Perez-Ramırez, Catal. Today, 119 (2007) 311.
[24] R. Quiceno, J. Perez-Ramırez, J. Warnatz and O. Deutschmann, Appl. Catal. A, 303 (2006) 166.
[25] P. Berlowitz, D.J. Driscoll, J.H. Lunsford, J.B. Butt and H.H. Kung, Comb. Sci. Technol., 40 (1984) 317.
[26] Y. Feng, J. Niiranen and D. Gutman, J. Phys. Chem., 95 (1991) 6558.
[27] M.B. Davis, M.D. Pawson, G. Veser and L.D. Schmidt, Combust. Flame, 123 (2000) 159.
[28] C.M. Marks and L.D. Schmidt, Chem. Phys. Lett., 178 (1991) 358.
[29] G.C. Eltenton, J. Chem. Phys., 15 (1947) 455.
[30] M. Sablier and T. Fujii, Chem. Rev., 102 (2002) 2855.
[31] G. Wannier, Phys. Rev., 90 (1953) 817.
[32] R.E. Winters, J.H. Collins and W.L. Courchene, J. Chem. Phys., 45 (1966) 1931.
[33] F.P. Lossing and G.P. Semeluk, Can. J. Chem, 48 (1970) 955.
[34] P. Plessis, P. Marmet and R. Dutil, J. Phys. B, 16 (1983) 1283.
[35] P. Plessis and P. Marment, Can. J. Chem, 65 (1987) 1424.
[36] H. Singh, J.W. Coburn and D.B. Gravesa, J. Vac. Sci. Technol. A, 18 (2000).
[37] http://webbook.nist.gov/chemistry.
[38] http://physics.nist.gov/PhysRefData/Ionization/molTable.html.
[39 http://discoverysciences.com/chromdb/default.aspx.
[40] P. Aghalayam, Y.K. Park, N. Fernandes, V. Papavassiliou, A.B. Mhadeshwar and D.G. Vlachos, J. Catal., 213 (2003) 23.
[41] C. Gueret, M. Daroux and F. Billaud, Chem. Eng. Sci., 52 (1997) 815.
[42] O. Olsvik, O.A. Rockstad and A. Holmen, Chem. Eng. Technol., 18 (1995) 349.
[43] K.L. Hohn, P.M. Witt, M.B. Davis and L.D. Schmidt, Catal. Lett., 54 (1998) 113.
[44] T. Ito, J.-X. Wang, C.-H. Lin and J.H. Lunsford, J. Am. Chem. Soc., 107 (1985) 5062.
[45] K.D. Campbell, E. Morales and J.H. Lunsford, J. Am. Chem. Soc., 109 (1987) 7900.
[46] S.N. Foner and R.L. Hudson, J. Chem. Phys., 25 (1956).
[47] S.S. Bharadwaj and L.D. Schmidt, Fuel Proc. Technol., 42 (1995) 109.
[48] F. Paneth and W. Hofeditz, Ber., 62B (1929) 1335.
[49] C.A. Mims, R. Mauti, A.M. Dean and K.D. Rose, J. Phys. Chem., 98 (1994) 13357.